Quantitative Evaluation of the Effects of Large-Scale Sea Wave Components on Microwave Backscattering From Ocean Surface

Dengfeng Xie and Feng Guo

***Abstract*—This article quantitatively examined the effect of these long-wave components with wavelength larger than the Bragg component on radar backscattering using the series-expanded first-order small-slope approximation (SSA-1) and the Hwang sea wave spectrum model. First, some roughness with various scales is constructed using different long-wave sea spectrum components and, subsequently, is cast into SSA-1 to obtain the corresponding normalized backscattering cross section (NBCS) at different radar frequency, incidence angles, and wind speeds, respectively. Then, the effect of large-scale wave components on radar backscattering is revealed by analyzing the NBCSs with different roughness. Finally, the existing wavelength filtering theory explained the effect of large-scale waves on radar backscattering. It was also verified by another scattering model, i.e., the advanced integral equation model and radar measurements. Besides, we also investigate the effects of sea states and swell waves on the numerical simulation results. The effect of long-scale waves on NBCS clarifies the source of backscattering from the multiscale sea surface, which is helpful for both analytical and numerical scattering models to explore the sea surface scattering properties and better interpret the radar sensing of sea surface. Also, the examination of the effect of sea states and swell waves on radar backscatter is instructive for reducing the inversion errors of sea surface wind speed from radar measurements by means of configuring the appropriate radar parameters (e.g., high frequencies and large-incidence angles).**

***Index Terms*—Bragg component, first-order small-slope approximation (SSA-1), multiscale roughness, radar backscattering.**

I. Introduction

ON LARGE undulating sea surface ride, many diverse scale harmonic waves bring the nature of sea surface with a multiscale roughness and a broad power spectrum [1], [2]. The small-scale waves of the sea surface are caused by local wind or arise due to the locally strong nonlinear processes (e.g., wave breaking events); and the air–sea interaction and the relatively weak nonlinear processes accumulating over vast areas are responsible for generating long waves [3]. Therefore, the multiscale feature leads to the complexity of the physical process involved in the interaction between electromagnetic (EM) waves and sea surface, especially in the microwave range where EM wavelength lies between the large gravity waves and the small capillary ripples [4]. Analytical or numerical scattering models play an important role in both the interpretation of the microwave scattering process from the sea surface and the retrieval of sea surface parameters [5]–[7]. The commonly used analytic models include classical Kirchhoff approximation (KA) and small perturbation model (SPM), and the unified models that bridge the gap between KA and SPM in the scope of application and are applicable to various scale roughness on sea surface within their respective theoretical frameworks, such as two-scale model (TSM), integral equation model (IEM) and its advanced version (AIEM), and a small-slope approximation (SSA) [8]–[13]. These scattering models are based on surface statistical parameters, e.g., normalized correlation function, correlation length, and root-mean-square (rms) height, which can be calculated using specific surface spectrum components [7]. These specific statistical input parameters of the scattering model represent a specific and identifiable roughness. Therefore, the resulting model outputs are only responsible for the specific roughness of a rough surface. That is to say, a set of input roughness parameters corresponds to the specific model output.

Wave scattering by the real sea surface, in fact, involves scattering at multiple scales [14]. It is known that the backscattering from small-scale waves is modulated by facet slopes because of the longer waves [10], [15]. The model-calculated scattering is a heuristic in one way or other in the sense that the boundary wavenumber has yet to be determined empirically, which obscures the details of the specific effect by different scale large waves on normalized backscattering cross section (NBCS). Xie *et al.* [16] discussed the effective roughness responsible for NBCS but did not cover the specific evaluation of the effect of long waves on radar backscatter. Besides, some numerical studies were devoted to exploring the effect of large-scale roughness on radar backscatter but they focused on a few large-scale roughness [17], [18]. Up to date, the more detailed quantitative evaluations of the effect of various long-scale wave components on NBCS are rarely reported. However, detailed knowledge of the contribution from different scale large waves is useful

Manuscript received 29 April 2022; revised 9 July 2022; accepted 15 July 2022. Date of publication 20 July 2022; date of current version 28 July 2022. This work was supported in part by the National Natural Science Foundation of China under Grant 42006158 and in part by the Natural Science Foundation of Jiangsu Province under Grant BK20200698. *(Corresponding author: Dengfeng Xie.)*

The authors are with the School of Geomatics Science and Technology, Nanjing Tech University, Nanjing 211800, China (e-mail: xiedfeng@njtech.edu.cn; gf3194918226@163.com).

Digital Object Identifier 10.1109/JSTARS.2022.3192556

This work is licensed under a Creative Commons Attribution 4.0 License. For more information, see https://creativecommons.org/licenses/by/4.0/

to reveal the underlying scattering mechanism and scattering source. In addition, it is instructive for the analytical TSM to determine the cutoff wavenumber for dividing large and small scales roughness. For the rigorous numerical methods, such as the method of moments [19], [20], the attempt is made to select on a basis to match the experimental data, the appropriate wave components to generate rough surface for calculating sea surface scattering. Although a rich body of research toward the radar response to sea surface roughness is available [21]–[27], the explicit effects of different scale long waves that control the radar response from the complex ocean waves are unclear. The knowledge of the effects from these long waves on radar backscattering is instructive to deepen our understanding of the process of EM waves from sea surface for extracting desired ocean variables (e.g., wind speed, wave height, wave slope, ocean–wave spectrum, and apparent surface temperature) from remote sensing of the ocean.

Based on the above requirement, this study attempts to quantitatively evaluate the effect of different large-scale waves of the sea surface on NBCS. The SSA scattering model can describe the scattering from both small- and large-scale surfaces within the single theoretical scheme and automatically taken into account the effect caused by the wave components at all scales inputted into the SSA model [28]–[30]. Considering the competence of SSA-1 model to cope with all scales wave components and its acceptable accuracy and efficiency in sea surface scattering simulations [31]–[33], the SSA-1 model is adopted in this study to simulate the NBCS from sea surface with different roughness. Therefore, to explore the effects of various large-scale waves on NBCS, we calculate the backscattering coefficients under different sea surface roughness with the SSA-1 model at various wind speeds and different radar frequencies in an effort to clarify the backscattering source from the multiscale sea surface. The rest of this article is organized as follows. Section II briefly introduces the SSA-1 and sea spectrum models. The numerical results of the effect of different large-scale waves on NBCS at different frequencies, incidence angles, and wind speeds are presented in Section III. In Section IV, we discuss more about the impact on the NBCS simulations. Finally, Section V concludes this article.

II. Methodology

When an incident plane EM wave $\hat{k}_i(\theta_i, \phi_i)$ along incidence angle θ_i and azimuth angle ϕ_i encounters a dielectric discontinuity at air–sea interface, a scattered wave $\hat{k}_s(\theta_s, \phi_s)$ with scattering angle θ_s and azimuth angle ϕ_s can be observed, whose amplitude is determined by the geometric and physicochemical properties of rough surface and the incident wave direction. The geometry of EM wave bistatic scattering from rough sea surface is illustrated in Fig. 1. Regarding the backscatter mode concerned in this study, there is $\hat{k}_s = -\hat{k}_i$.

A. First-Order SSA Model

The incoherent normalized radar cross section calculated by using the SSA-1 model is expressed as follows [29], [30], [34], [35]:

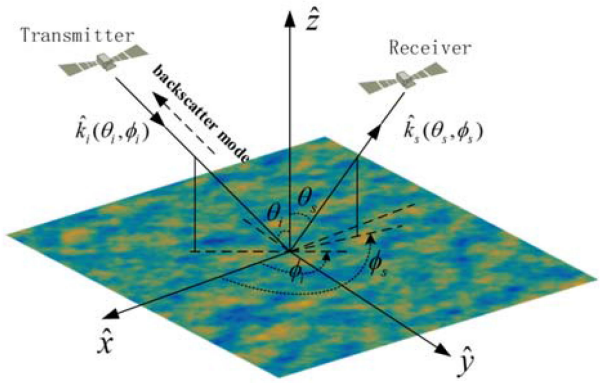

Fig. 1. General geometry of EM wave scattering from rough sea surface. (The colors of base diagram represent different sea elevations.).

$$\sigma_{pq}^{0}(\mathbf{k}_i, \mathbf{k}_s) = \frac{1}{\pi}\left|\frac{2q_i q_s B_{pq}(\mathbf{k}_i, \mathbf{k}_s)}{Q}\right|^2 \cdot \int \exp\left(-\sigma_z^2 Q^2\right) \cdot \left\{\exp\left[\sigma_z^2 Q^2 \rho(\mathbf{r})\right] - 1\right\} \cdot \exp\left[j\left(\mathbf{k}_s - \mathbf{k}_i\right) \cdot \mathbf{r}\right] d\mathbf{r} \quad (1)$$

where the subscripts q and p denote the received and transmitted polarizations, respectively; $\{\mathbf{k}_i, \mathbf{k}_s\}$ are the horizontal projections of the incident and scattered wave vectors, and $\{q_i, q_s\}$ are their vertical projections, respectively. $Q = q_i + q_s$. $B_{pq}(\mathbf{k}_i, \mathbf{k}_s)$ is the matrix of the first-order small perturbation method given in [29]; σ_z^2 and $\rho(\mathbf{r})$ are the variance and autocorrelation function of the sea surface, respectively.

In this study, the Bragg wavenumber is used as the reference for measuring different large-scale waves. To examine the effect of large-scale waves with wavelength larger than the Bragg components on radar backscatter, we rewrite (1) in terms of the sea wave spectrum. After some lengthy but straightforward manipulations, (1) can be expressed with different order sea wave spectrum as a compact form [35]

$$\sigma_{pq}^{0}(\mathbf{k}_i, \mathbf{k}_s) = 4\pi\left|\frac{2q_i q_s B_{pq}(\mathbf{k}_i, \mathbf{k}_s)}{Q}\right|^2 \cdot \exp\left(-\sigma_z^2 Q^2\right) \sum_{n=1}^{\infty} \frac{\left(\sigma_z^2 Q^2\right)^n}{n!} W^{(n)}\left(\mathbf{k}_s - \mathbf{k}_i\right) \quad (2)$$

with

$$W^{(n)}(\mathbf{k}_s - \mathbf{k}_i) = \frac{1}{(2\pi)^2}\int_0^{\infty}\int_0^{2\pi} \rho^n(\mathbf{r}) \cdot \exp\left[j(\mathbf{k}_s - \mathbf{k}_i) \cdot \mathbf{r}\right] d\mathbf{r} \quad (3)$$

where $W^{(n)}$ is the higher order sea wave spectrum and can be expressed as the Fourier transform of the nth power of the two-dimensional (2-D) normalized correlation function of rough sea surface $\rho^n(\mathbf{r})$. The detailed manipulations can also be seen in the Appendix.

The vector $\mathbf{k}_s - \mathbf{k}_i$ in (3) has the following form in rectangular and polar coordinates, respectively:

$$(\mathbf{k}_s - \mathbf{k}_i) = (k_{sx} - k_{ix}, k_{sy} - k_{iy}) = (K, \phi) \tag{4}$$

with

$$k_{sx} = k \sin\theta_s \cos\phi_s, \quad k_{sy} = k \sin\theta_s \sin\phi_s \tag{5a}$$

$$k_{ix} = k \sin\theta_i \cos\phi_i, \quad k_{iy} = k \sin\theta_i \sin\phi_i \tag{5b}$$

$$K = \sqrt{(k_{sx} - k_{ix})^2 + (k_{sy} - k_{iy})^2} \tag{5c}$$

$$\phi = \arctan\left(\frac{k_{sy} - k_{iy}}{k_{sx} - k_{ix}}\right) \tag{5d}$$

where k is the EM wavenumber, K represents a specific spectrum component of rough sea surface, which is called "Bragg component," K_{Bragg}, and ϕ describes the azimuth direction of the corresponding Bragg component relative to the upwind direction. In backscattering ($\theta_i = \theta_s$, $\phi_s = \phi_i + \pi$), K is equal to $2k \sin\theta_i$ ($0^\circ \le \theta_i \le 90^\circ$). Hence, the higher order sea wave spectra at the Bragg component K_{Bragg} along the azimuthal direction ϕ relative to upwind direction contributes to the NBCS [36]. For more details about SSA-1 model and the parameters therein, readers are referred to [29], [30], [34], and [35].

B. Sea Wave Spectrum Model

To drive the SSA model, we need a quantitative description of sea surface roughness, i.e., normalized autocorrelation function and rms height. For sea surface under the Gaussian assumption, many sea spectrum models are developed to describe the undulating sea surface in terms of energy. A 2-D directional sea spectrum is expressed as the product of two parts: one is the omnidirectional spectrum $S(K)$ representing the isotropic part, and the other is the angular spreading function $\Phi(K, \phi)$ [2] and is given in polar coordinates as follows:

$$S(K, \phi) = \frac{1}{K} S(K) \Phi(K, \phi) \tag{6}$$

where

$$\Phi(K, \phi) = [1 + \Delta(K) \cdot \cos(2\phi)]/2\pi. \tag{7}$$

In (6), ϕ is the azimuth angle relative to mean wind direction in the frequency domain; and in (7), $\Delta(K)$ is the upwind–crosswind ratio that describes the anisotropy of the spreading function [2]. The mean square height σ_z^2, mean square slope σ_s^2, and normalized autocorrelation function $\rho(r, \varphi)$ of sea surface elevation are related to the sea wave spectrum by

$$\sigma_z^2 = \int_0^\infty S(K) dK \tag{8}$$

$$\sigma_s^2 = \int_0^\infty K^2 S(K) dK \tag{9}$$

$$\rho(r, \varphi) = \frac{1}{\sigma_z^2} \int_0^\infty \int_0^{2\pi} S(K, \phi) \exp(jKr \cos(\varphi - \phi)) K dK d\phi \tag{10}$$

where φ is the azimuth angle relative to the upwind direction in the spatial domain, and r is the lag distance along the azimuth direction φ. The integrand, $K^2 S(K)$, in (9) is called the slope spectrum [2].

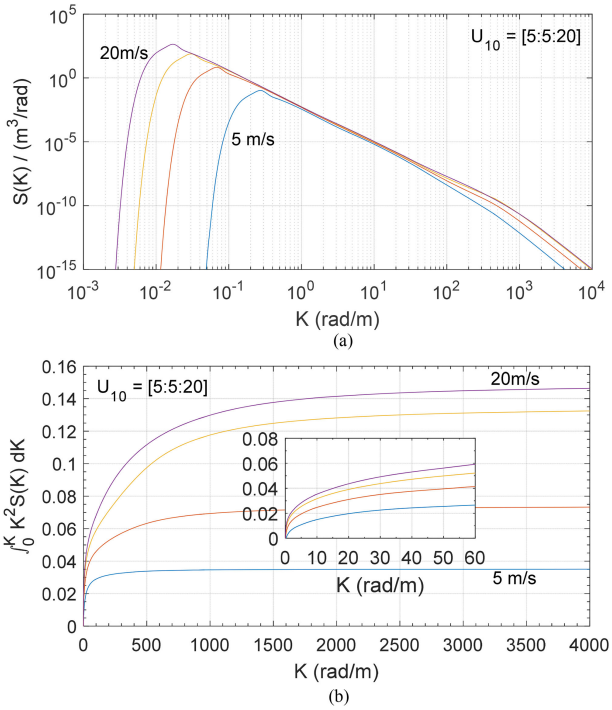

Fig. 2. (a) Omnidirectional H18 sea wave spectrum $S(K)$ and (b) cumulative mean square slopes at several wind speeds ranging from 5 to 20 m/s with the interval of 5 m/s.

The newly developed Hwang spectrum [37], labeled as H18 spectrum hereafter, is adopted to drive the scattering model due to its robustness in the simulations of NBCS from sea surface [37]–[39]. The H18 spectrum combines the H15 [25] in the high-frequency region ($K > 1$ rad/m) and the G spectrum [38] in the low-frequency region ($K \le 1$ rad/m), and the spectrum in the region between $1 \le K \le 4$ rad/m is linear interpolated. The omnidirectional H18 spectrum of fully developed seas (i.e., the inverse wave age of sea waves is 0.84), $S(K)$, and the cumulative mean square slopes (i.e., $\int_0^K K^2 S(K) dK$) [2], at the wind speeds of 5–20 m/s with the interval of 5 m/s, are plotted in Fig. 2. Here, the specific variables in H18 spectrum are referred to that in its MATLAB code [37].

It can be seen in Fig. 2(a) that, as wind speed increases, the peak of height spectrum shifts to lower wavenumber, and the energy of each spectrum component increases. Meanwhile, most of the energies of sea surface waves are mainly occupied by low-frequency components, which determine the rms height of the sea surface [see (8)]. In Fig. 2(b), the cumulative mean square slope has a similar variation with wind speed to that of the height spectrum, and the contributions from different wave components to the mean square slope reduce as the wavenumber of wave component increases, especially for low wind speed.

III. Numerical Results

In this section, we show the numerical NBCSs with and without the large-scale waves relative to Bragg wave component

in the execution of SSA-1 model at several incidence angles, wind speeds, and radar frequencies, respectively. By comparative analysis of these simulations, the quantitative effect of large-scale waves on radar backscattering will be made clear.

From the SSA-1 model in (2)–(5), we see that it is the surface spectrum with different orders, $W^{(n)}(K,\phi)$, evaluated at Bragg resonant components K_{Bragg} in the azimuth of ϕ that produces backscattering [11], [29]. Therefore, the Bragg component K_{Bragg} is entailed in the generation of roughness scales. Now, we construct various roughness generated by wave components containing different large-scale wave components relative to the Bragg component. Based on this, the range of the spectrum components used for constructing the sea surface roughness is $[cK_{\text{Bragg}},\infty)$, where c is a nonnegative variable parameter with the maximum value of 1. Thus, the long wave component participating the construction of roughness can be controlled by adjusting the parameter c. The above experimental setup enables us to examine the effect of large-scale waves with wavelength larger than the Bragg component in radar backscattering. Accordingly, the lower limit of wavenumber variable K in the integrals in (8)–(10) is replaced by cK_{Bragg}.

In this study, the values of $c$are taken between 0 and 1 at the interval of 0.02. When c is close to 0, it corresponds to the case that the full-spectrum components participate in the construction of sea roughness, which involves the effect of all scale waves on radar backscattering. The radar parameters in this study focus on the low-frequency L-band ($f = 1.26$ GHz and $k =$ 26.34 rad/m) and medium-frequency C-band ($f = 5.3$ GHz and $k = 111$ rad/m), and the incidence angles varying from normal incidence to 70°. The wind speed representing sea condition is set to be within 20 m/s. Also, the Debye equation [40] is applied to obtain the seawater permittivity with fixed seawater temperature and salinity at 20 °C and 35 ppt. Based on the above parameters, the corresponding NBCSs calculated by the SSA-1 model are given next.

A. Incidence Angle Dependence

We simulated the L-band copolarized NBCSs varying with variable c ranging from 1 to 0 at several incidence angles along the azimuth in line with the upwind direction, assuming that the wind speed is 10 m/s. The corresponding simulations are shown in Fig. 3.

In Fig. 3, we see that, at near-normal incidence, the Bragg component K_{Bragg} in 5(c) equal to $2k\sin\theta_i$ is very close to 0 rad/m, which indicates that most of the long wave components are responsible for sea surface roughness, whatever the value of c is. The full-spectrum component generates a large-scale roughness with the correlation length up to more than 10 m and the rms height up to tens of centimeters at a wind speed of 10 m/s [18], [34]. In this case, the scattering characteristic follows the behavior of KA model and has no difference in polarization [6].

As incidence angle increases to medium angles (e.g., within 30°), the large-scale gravity wave components significantly affect NBCSs. For example, at an incidence angle of 10°, the effect of large-scale wave components causes a difference of

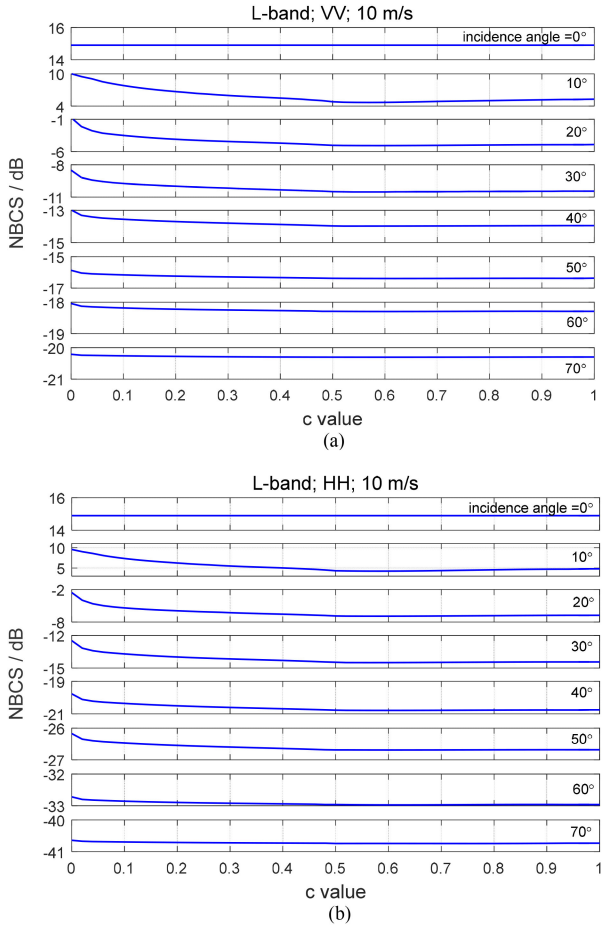

Fig. 3. Simulated L-band NBCSs for (a) VV-polarization and (b) HH-polarization versus *c-values* at upwind direction with the wind speed of 10 m/s for several incidence angles ranging from normal incidence to 70°.

about 5 dB. The differences are about 4 and 3 dB for incidence angles of 20° and 30°, respectively. Besides, one can see that these large-scale waves with noticeable effect on NBCSs concentrate on the range from 0 to $0.5K_{\text{Bragg}}$, while other scale waves larger than the Bragg component have little influence on radar backscattering. The reason is because, taking the incidence angle of 30° an example, the wavenumber of Bragg component ($2k\sin\theta_i$, here, $\theta_i = 30°$) in this case is equal to the wavenumber of L-band, i.e., 26.34 rad/m, and the lower limit (i.e., cK_{Bragg}) of wave components participating the generation of sea surface roughness for NBCS simulations is greater than 13.17 rad/m after c-value exceeds 0.5.

It can be seen from Fig. 2(b) that about half of the mean square slope of sea surface under wind speed of 10 m/s is contributed by these wave components with a wavenumber less than 13.17 rad/m. However, the effect of large-scale waves on radar backscattering is carried out by the slope of the sea surface, which changes the local incidence angle of EM waves. Therefore, these wave components with relatively small contribution to the slope of sea surface also have the limited effect on radar backscattering at L-band.

When incidence angle increases further, say, greater than 50°, the effect of the long waves on radar backscattering becomes

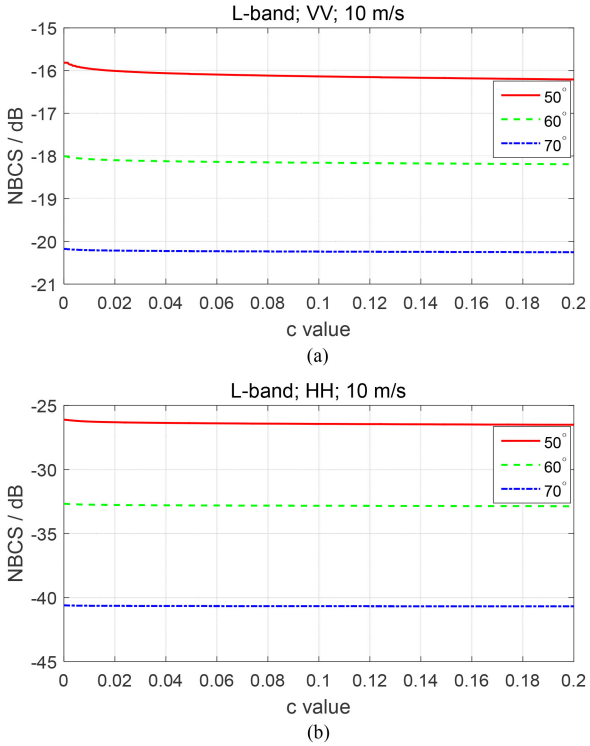

Fig. 4. Similar to Fig. 3 but for more nuanced segmentation of the c-value ranging from 0 to 0.2 with the interval of 0.0005.

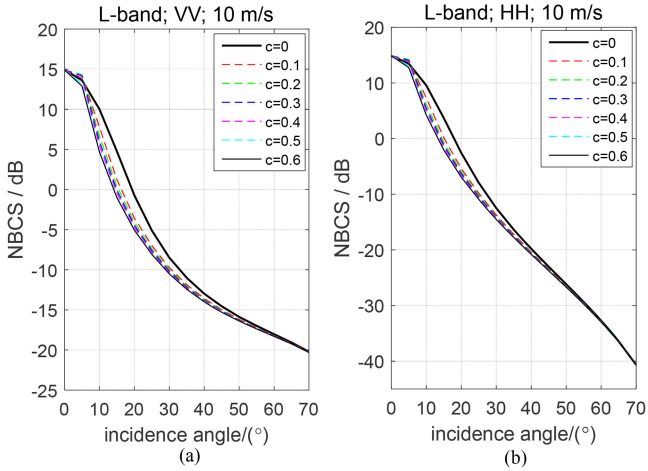

Fig. 5. NBCSs for (a) VV-polarization and (b) HH-polarization from Fig. 3 but replotted in function of incidence angle for several different *c-values*.

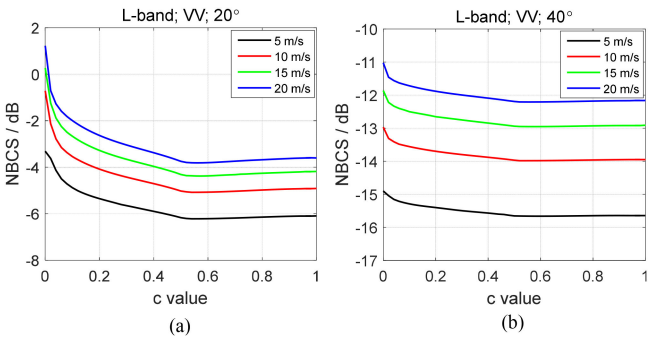

Fig. 6. VV-polarized NBCSs varying with *c-value* for several wind speeds at incidence angels of (a) 20° and (b) 40°.

weaker and weaker, which is within about 1 dB and even almost disappears at incidence angle up to 70°. It indicates that only the small-scale sea waves are responsible for radar backscattering at large-incidence angles. The Bragg wavenumber at the incidence angle of 70° is relatively large up to 49.6 rad/m. When the c-value increases by one interval length from zero, i.e., $c = 0.02$, the corresponding lower limit of the range of these wave components used for generating the sea surface roughness is about 1 rad/m. However, these wave components with wavenumber less than 1 rad/m have relatively large contribution to mean square slope. To further examining the effect of these wave components with wavenumber less than 1 rad/m on radar backscattering at large-incidence angles, it requires a more nuanced segmentation of the c-value. In this case, similar to Fig. 3, we replot the NBCSs versus c-value but ranging from 0 to 0.2 with the interval of 0.0005 for incidence angles of 50°, 60°, and 70°, as shown in Fig. 4.

It is clearer to show the effect of large-scale waves with the wavenumber ranging from 0 to $0.2K_{\text{Bragg}}$ on radar backscattering at large-incidence angles. These simulations further demonstrate that the large-scale long waves on sea surface still have little effect on radar backscattering at large-incidence angles.

Besides, to show the effect of large-scale waves on NBCS more clearly, we replot the variations of NBCS with incidence angles for several different *c-values,* as shown in Fig. 5. It shows that the largest wave components ranging from 0 to $0.1K_{\text{Bragg}}$ have the most significant impact on radar backscattering and continue so up to incidence angle of 50°. Beyond 50°, these large-scale wave components have little effect on radar backscattering. However, the influence from other large-scale wave components except for these components ranging from 0 to $0.1K_{\text{Bragg}}$ on the sea surface gradually decreases and is unchanged when the c-value exceeds 0.5.

In short, the large-scale wave components with wavenumber between 0 rad/m and $0.5K_{\text{Bragg}}$ have different degrees of effect on radar backscattering for incidence angles less than 50°. However, these large-scale wave components have little effect on NBCSs for incidence angles greater than 50°. The numerical results verified that these large-scale wave components can be ignored in calculating the NBCSs at medium- and large-incidence angles [14].

B. *Wind Speed Dependence*

The wind speed is a factor that shapes the sea wave spectrum, which represents the energy distribution of each wave component [see Fig. 2(a)]. Therefore, it is necessary to investigate the effect of large-scale wave at different wind speeds. Here, based on the analysis in Section III-A, we select a small-incidence angle of 10° and a moderate incidence angle of 40° to examine the impact of the wind speed on the effect of large-scale waves on VV-polarized NBCS. The simulation results at different wind speeds are shown in Fig. 6.

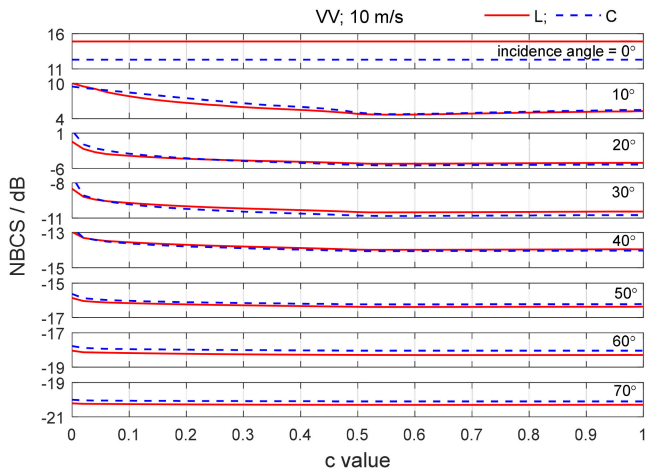

Fig. 7. Similar to Fig. 3 but with a comparison between *L*- and *C*-bands.

We can see in Fig. 6 that, for the two incidence angles, the difference between the NBCSs at $c = 0$ and $c = 1$ becomes large with the increase of wind speed, indicating that the effect of large-scale waves on NBCSs is more significant for higher wind speed. This is because these large-scale wave components also have large contribution to sea surface slope with the increase of wind speed [see Fig. 2(b)]. While the variation trends of NBCS with *c*-value are consistent with each other regardless of wind speed, their difference mainly exists in the levels of radar backscattering. A similar behavior at different wind speeds suggests that the effect of long-scale wave on radar backscattering not only affected by wind speed but only related to wave components used in the calculation for a given radar frequency.

C. Radar Frequency Dependence

Unlike the wind speed, the frequency will change the wave components inputted into SSA-1 for each calculation of NBCS simulation. To investigate the effect at different radar frequencies, we also calculated *C*-band ($f = 5.3$ GHz and $k = 111$ rad/m) radar backscattering at different incidence angles, similar to the treatment of *L*-band. The corresponding simulations for VV-polarization are displayed in Fig. 7.

It can be seen from Fig. 7 that the NBCSs at *L*- and *C*-bands have a similar behavior varying with the *c*-value, although they correspond to different sea spectrum components. For incidence angles within 30°, these large-scale wave components with significant effect on NBCS at *C*-band still range from 0 to $0.5K_{\text{Bragg}}$, which is similar to that at *L*-band. As the incidence angle increases, the effect of large-scale wave components on NBCS is very weak and even vanishes at incidence angle of 70°. A similar variation of the effect on radar backscattering with *c*-value for different radar frequencies indicates that the sizes of these large-scale wave components with significant effect on radar backscattering are relative. They only relate to respective Bragg resonant components K_{Bragg} ($K_{\text{Bragg}}=2k\sin\theta_i$). This phenomenon is elaborated in Section IV.

IV. Discussion

A. Explanation of the Effects of Large-Scale Waves on NBCS

Based on the aforementioned numerical results, we find that the long waves larger than the Bragg component has a different effect on NBCSs with incidence angles. This phenomenon can be physically explained by "the wavelength filtering effect" [36]. According to Bragg resonance theory [41], [42], when an EM wave with a wavelength λ impinging on the sea surface at the incidence angle of θ_i, the sea wave component with the wavelength equal to $\lambda/(2\sin\theta_i)$ causes the resonance in backscattering. In essence, the resonance sea wave wavelength corresponds to the Bragg wavenumber K. Here, we introduce the concept of radar "effective wavelength," λ_e, as reported in [36], equal to the resonance wavelength, i.e., $\lambda_e = \lambda/(2\sin\theta_i)$. The wavelength filtering suggests only those roughness scales comparable to the effective wavelength contribute to the backscattering, rationalized by the fact that the smaller roughness cannot induce backscattering due to its small size, while the larger roughness serve as a reference plane for scattering. Readers can refer to [36] for more details about the concept of wavelength filtering.

As an illustrative purpose, Fig. 8(a) shows the *L*-band effective wavelength varying with incidence angles with the red solid line. The surface roughness is characterized by the correlation length and rms height. Therefore, to compare with effective wavelength, the correlation length of different scale roughness generated by using a portion of large-scale wave components with wavelength larger than that of Bragg components is also shown in Fig. 8(a). Besides, the other roughness parameters, such as correlation function, rms height, and rms slope, are plotted in Fig. 8(b)–(d), respectively.

In Fig. 8(a), the effective wavelength is very large at an incidence angle of about 0° (it is not plotted in the figure because of its infinite value). In this case, all wave components are used to generate a large-scale rough surface with a correlation length up to 14.5 m [see Fig. 8(a) and (b)] and rms height of about 0.65 m [see Fig. 8(c)]. At incidence angles less than 30°, the corresponding effective wavelength is relatively large, and these large-scale wave components still contribute to radar backscattering. As the incidence angle increases further (i.e., larger than 40°), the effective wavelength becomes smaller and smaller. The influence of large-scale wave components on radar backscattering also becomes weaker and weaker because the roughness of large-scale waves is gradually away from the effective wavelength. In this case, the large-scale waves have to be excluded as the scattering source by the wavelength filtering and only serve as the reference plane for small-scale waves. For example, at large-incidence angles (e.g., greater than 50°), the correlation length of small-scale roughness is much closer to the corresponding effective wavelength. So, it is selected as the source responsible for radar backscattering.

The correlation function of sea surface bears zero crossings [see Fig. 8(b)], given rising from the fact that the wave spectrum starts from zero and reaches a maximum value at low wavenumber [34], [43]. Moreover, the correlation function of a

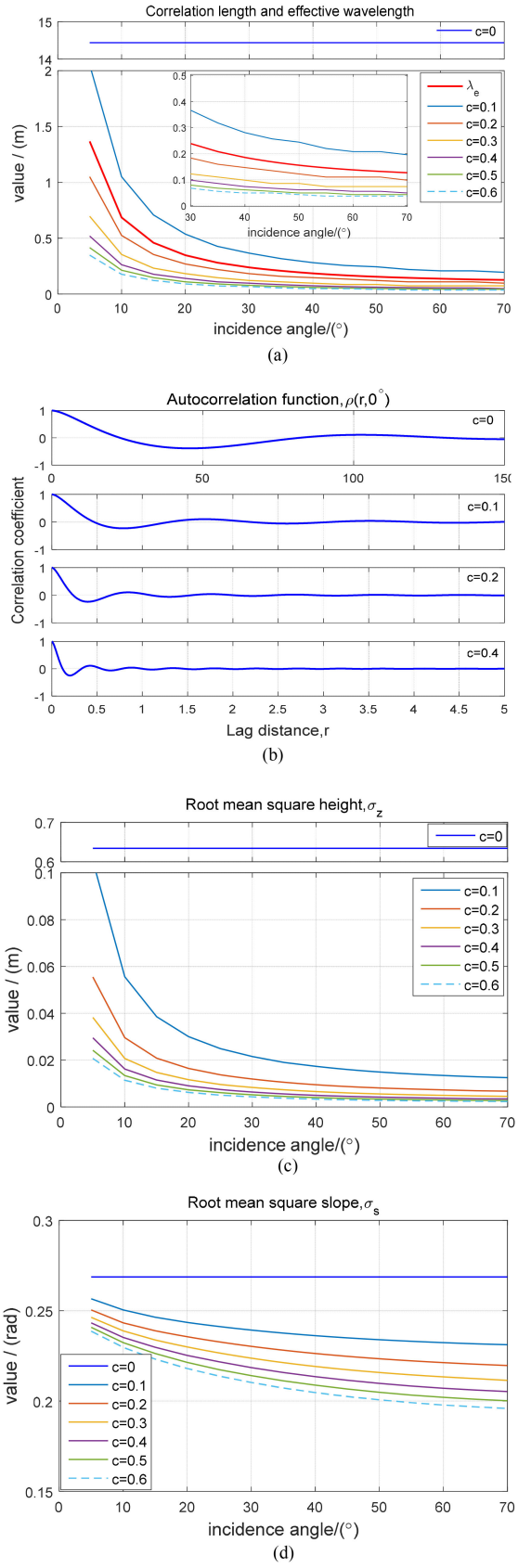

Fig. 8. Related roughness parameters at *L*-band with the wind speed of 10 m/s in upwind direction for (a) effective wavelength and correlation length, (b) normalized autocorrelation function, (c) rms height, and (d) rms slope.

smaller scale roughness has more zero crossings before decaying to zero, which is in accord with the experimental results of short wind wave fields derived from the wave profiles captured by a high-resolution camera [45], Fig. 13.

In Fig. 8(c) and (d), we find that the rms height and rms slope of roughness are proportional to the size of the roughness. These large-scale waves exist within the radar antenna illuminated area and modulate the small-scale roughness by large surface slope for multiscale sea surface. However, they are filtered out by effective wavelength and have little effect on radar backscattering at large-incidence angles (e.g., greater than 50°). Therefore, heuristically including these large-scale waves in modeling will generate an error or misrepresent the cause of scattering.

B. Validation by AIEM and Radar Measurements

To further look into the effect of large-scale waves on radar backscattering, an AIEM model was used to cross verify this effect. In this section, we simulated the upwind-direction NBCSs at *L*- and *C*-bands using SSA-1 and AIEM models with the wind speed of 10 m/s when the *c*-value is set to be 0 and 0.5, respectively. The validation data adopted in this text come from Aquarius radar extracted from [17] and [45] for *L*-band and from the experimental *C*-band geophysical model function (CMOD7) (no HH-polarization) [46] for *C*-band. The Aquarius radar only had three incidence angles of 28.7°, 37.8°, and 45.6°. The CMOD7 geophysical model function (GMF) model is available from the Royal Netherlands Meteorological Institute (KNMI), and the suggested incident angles are from 16° to 66°. The corresponding comparisons between them are shown in Fig. 9.

We can see from Fig. 9 that the NBCSs simulated by SSA-1 and AIEM models using full-spectrum components (i.e., $c = 0$) are the same for both *L*- and *C*-bands at near-normal incidence. The difference of NBCS calculated by using the two models is negligible until the incidence angle reaches about 30° except for *L*-band VV-polarizations. For incidence angles between 30° and 50°, the large-scale wave components ranging from 0 to $0.5K$ rad/m still contribute to NBCSs and cannot be omitted entirely. However, their effect becomes weaker and weaker. With the increase of incidence angles, the scattering sources gradually move toward the small-scale wave. Here, if we still use these large-scale wave components in the AIEM model, the estimated NBCS results have a large error. As for why the SSA model is not affected by these large-scale waves at large-scale incidence angle, we may view from the fact that the SSA model is derived from the slope of the rough surface and is dominated by rms slope of rough surface [13], while AIEM model is based on surface fields and their behavior is controlled by the correlation length and rms height of surface [11], [12]. This distinction between derivation basis results in different kernels in scattering amplitudes [5], which causes the difference in applicability of the two models. After the incidence angle greater than 50°, the calculated results by SSA-1 with (i.e., $c = 0$) and without (i.e., $c = 0.5$) these large-scale wave components and by AIEM without (i.e., $c = 0.5$) these large-scale waves are very close to each other and are good agreement with reference data. It indicates, at these

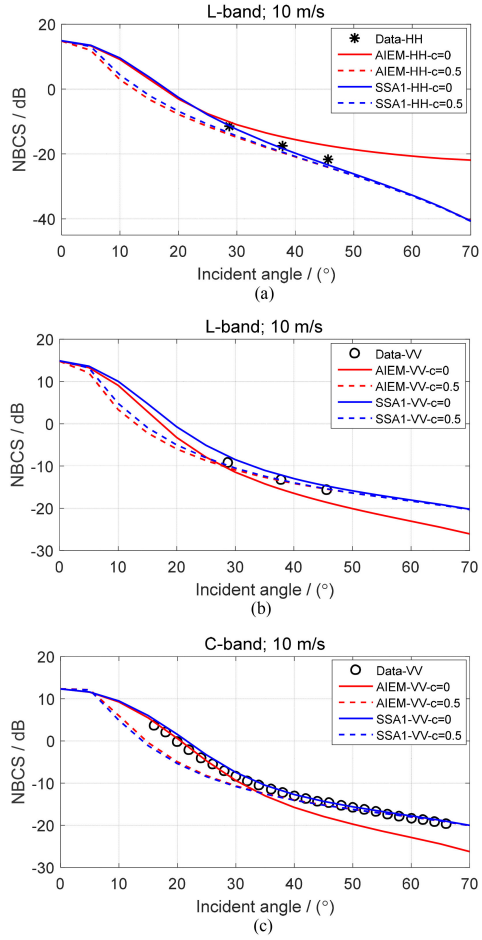

Fig. 9. Comparisons of NBCSs calculated by SSA-1 and AIEM at upwind direction with wind speed of 10 m/s with reference data coming from Aquarius radar for (a) *L*-band HH-polarization and (b) *L*-band VV-polarization, and from CMOD7 (no HH-polarization) for (c) *C*-band VV-polarization.

large-incidence angles, it cannot blindly add these large wave components into the AIEM model. Otherwise, it will result in a large error.

C. Uncertain Considerations of the Simulation Results

All the previous results are simulated under the assumption of fully developed sea state with inverse wave age of $\Omega = 0.84$. Henceforth, the sea state in this article refers to the development of sea waves described by using the parameter of inverse wave age. In the real ocean, however, the fully developed sea state is rare due to the limits of wind fetch [47]. So far, many research articles have investigated the effect of sea states on the sea surface roughness and radar scattering, e.g., [2] and [48]–[51]. To further examine the effect of sea states on the simulations in this article, we continue to conduct a similar numerical simulations to these in Section III but with different sea states. Fig. 10 shows the H18 wind wave spectrum varying with the inverse wave ages of 0.84, 1.5, and 2 when the wind speeds are 5, 10, and 15 m/s.

It can be seen from Fig. 10 that the sea state only affects the power levels of large-scale wave components but almost have no effect on the short-wave components for different wind

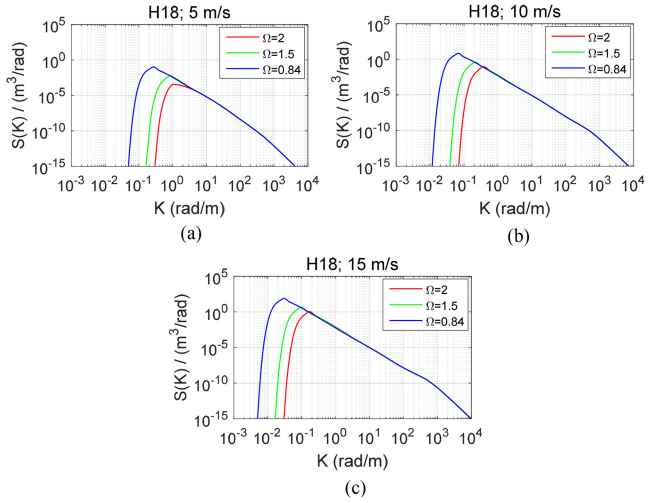

Fig. 10. Effects of sea states (i.e., inverse wave ages) on H18 wind wave spectrum versus the wavenumber K at wind speeds of (a) 5 m/s, (b) 10 m/s, and (c) 15 m/s.

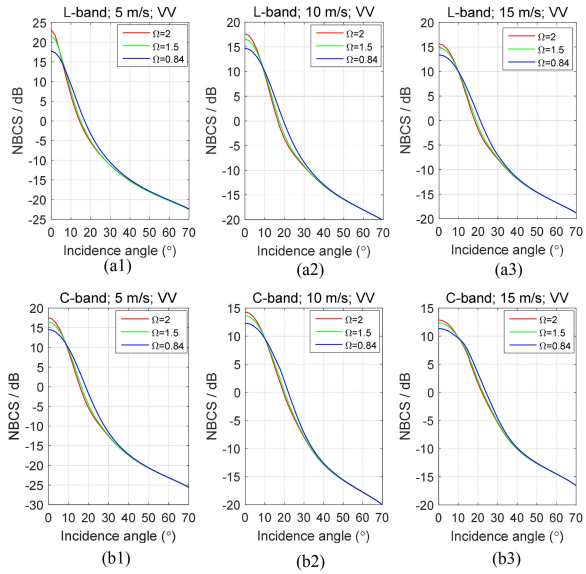

Fig. 11. Effect of sea states on the upwind-direction NBCS simulations in terms of incidence angles at wind speeds of 5 m/s, 10 m/s, and 15 m/s for (a) *L*-band and (b) *C*-band, respectively.

speeds. According to the analysis in Section III-A, the sea states should only have an influence on the NBCSs simulated at small- and medium-incidence angles. To verify this, we simulated the NBCSs in terms of incidence angles at *L*- and *C*-bands by using the full-wave components of wind wave spectrum under the sea states corresponding to Fig. 10, respectively. The simulation results are shown in Fig. 11.

We can see from Fig. 11 that the sea state has the varying degrees of influence on NBCS simulations for different incidence angles. On the whole, the influence is obvious within the incidence angles less than 30°. For small-incidence angles less than about 10°, the large-scale waves dominate the backscattering so that the sea state has a large influence on the NBCS simulations. For example, under the case of low wind speed of 5 m/s and *L*-band with the vertical incidence [see Fig. 11(a1)], the effect

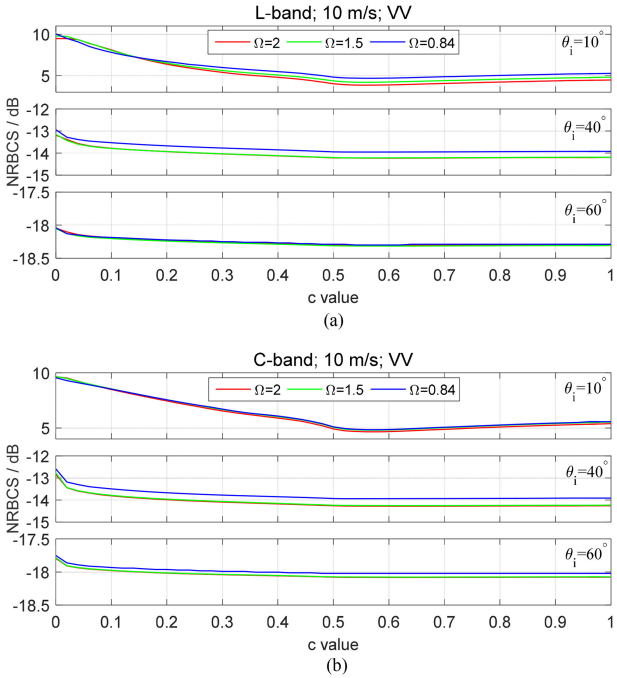

Fig. 12. Simulated VV-polarized NBCSs varying with c-values under the three sea states with inverse wave ages of 2, 1.5, and 0.84 for different incidence angles at (a) L- and (b) C-bands when the wind speed is 10 m/s.

on NBCS can reach to about 5 dB. The effect becomes small with the increases of incidence angles, wind speeds, and radar frequencies [see Fig. 11(a1)–(a3) and (b1)–(b3)]. Besides, when the sea state tends to be fully developed, the simulated NBCSs at incidence angles within 10° decrease. This is because the roughness of sea surface becomes large when the sea tends to be fully developed, which can reduce the power levels of backscattering at the vicinity of vertical incidence; while, the backscattering at incidence angles within about 10° to 40° increases as the sea surface becomes rougher. After the incidence angle exceeds 40°, the sea states have almost no effect on radar backscattering. As mentioned in the pieces of literature, e.g., [49] and [52], the sea state is an important factor to be considered when we use the information obtained from altimeter to retrieve the geophysical parameters of sea surface.

In summary, the sea state only affects the power levels of large-scale wave components, resulting in some influence on the values of NBCSs simulated at small- and medium-incidence angles where the large-scale wave components have varying modulation impacts on radar backscattering through their tilting effects. To further investigate the modulation effect by different large-scale wave components under various sea states on radar backscattering at different incidence angles, we follow the same strategy as that in Section III-A through comparing the NBCSs contributed by a portion of large-scale wave components with the wavelength larger than that of Bragg component with those simulated based on the full-wave components. The corresponding VV-polarized simulation results at incidence angles of 10°, 40°, and 60° for L- and C-bands under the wind speed of 10 m/s are shown in Fig. 12.

In Fig. 12, one can be seen the variation trends of the simulated NBCSs versus c-values are the same regardless of the sea states and radar frequencies, which accords to Figs. 3 and 7 but differs in the levels of NBCSs simulated at $c = 0$. That is, the sea states do not affect the variation trend of modulation effects by the large-scale wave components on the radar backscattering at different incidence angles but only with a small movement up or down along the NBCS axis.

In addition to the influence of sea states on the large-scale wave components, the swell waves coming from far away can also affect the large-scale low-frequency wind wave components, which often results in a multipeaked sea wave spectrum [53]. Many investigations indicate that the swell waves have a noticeable effect on radar backscattering and the inversion accuracy of sea surface parameter [54]–[56], especially for using the altimeter instruments [57], [58]. Among them, Durden and Vesecky [54] had numerically investigated the effect of swell waves on radar backscattering at various wind speeds, incidence angles, and radar frequencies, and they conclude that the swell waves have a significant effect on the radar backscattering at low frequencies (L-band) and small-incidence angles and have almost no influence for high frequencies (e.g., Ku-band) with large-incidence angles. This conclusion is consistent with the influences of sea states on radar backscattering mentioned above analysis. To examine the effect of swell waves on the NBCS simulations, we considered the swell effect in the following simulations. Here, a simple swell spectrum adopted in [54] is used, which is modeled as a narrow-band Gaussian process with the following expression:

$$\Psi_{\text{swell}}(K_x, K_y) = \frac{\langle h^2 \rangle}{2\pi\sigma_{K_x}\sigma_{K_y}} \exp\left\{-\frac{1}{2}\left[\left(\frac{K_x - K_{xm}}{\sigma_{K_x}}\right)^2 + \left(\frac{K_y - K_{ym}}{\sigma_{K_y}}\right)^2\right]\right\} \tag{11}$$

where $\langle h^2 \rangle$ is the variance due to the swell; K_{xm} and K_{ym} are the x- and y-components of the wavenumbers of spectral peak, respectively; and σ_{K_x} and σ_{K_y} are the standard deviations of K_x and K_y about K_{xm} and K_{ym}, respectively. In general, the standard deviations are both small.

In the following numerical simulations, we use the same swell parameters as in [54], i.e., $\sigma_{K_x} = \sigma_{K_y} = 0.0025$; the wavelength of swell wave is 300 m, and the rms height of swell is 4 m. Assuming that swell waves with these parameters propagate in the radar look direction. Fig. 13 shows the simulated NBCSs at different incidence angles along the upwind direction from the fully developed seas (i.e., $\Omega = 0.84$) with and without consideration of the swell effect at wind speeds of 5 m/s and 15 m/s for L- and C-bands, respectively.

We can see from Fig. 13 that the swell waves have a remarkable influence on the radar backscattering at small- and medium-incidence angles. For incidence angles larger than 50°, the swell waves have a negligible effect on NBCS simulations. Besides, the effect becomes relatively small as the wind speeds and radar frequencies increase. To examine the effect of swell waves on the modulation by large-scale waves on the NBCS

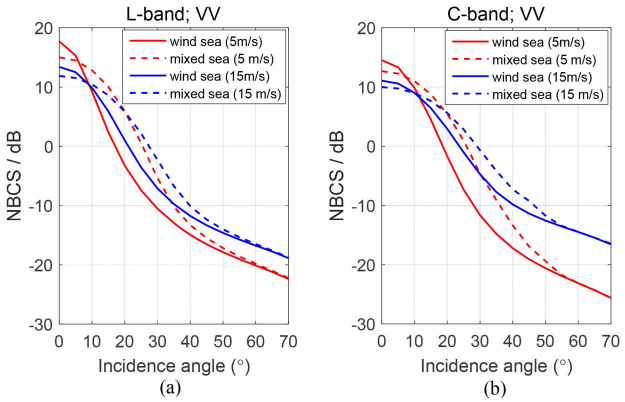

Fig. 13. Simulated VV-polarized NBCSs in terms of incidence angles along the upwind direction from the fully developed wind sea at wind speeds of 5 m/s and 15 m/s and from the corresponding mixed sea with a swell wave having the wavelength of 300 m and the rms height of 4 m for (a) *L*-band and (b) *C*-band, respectively.

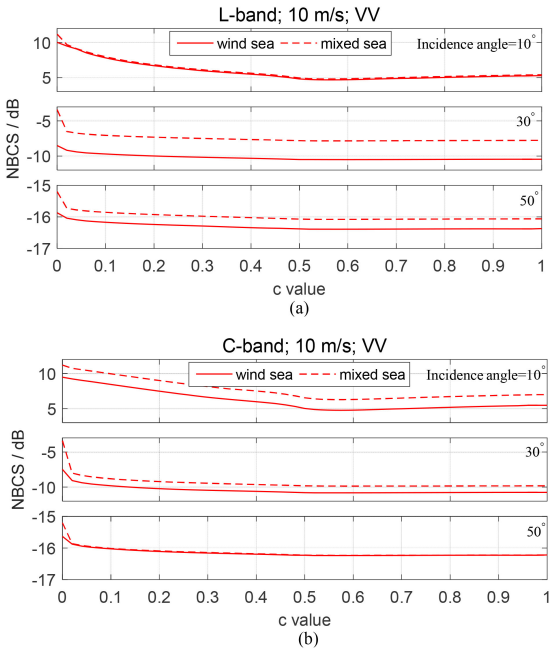

Fig. 14. Similar to Fig. 12 but under the scenarios of fully developed sea and its mixed seas with the Gaussian swell waves expressed in (11).

simulations, we simulate the NBCSs under different large-scale waves for several incidence angles, which is similar to Fig. 12, but with one scenario change from the sea state to the swell wave. The corresponding simulation results are shown in Fig. 14.

It can be seen from this figure that the effect of swell waves on the modulation by different large-scale wave components on simulated NBCSs at different incidence angles are similar to that of sea states (see Fig. 12). That is, these large-scale wave components with wavenumber less than $0.5K_{\text{Bragg}}$ have relatively large effect on radar backscattering at small- and medium-incidence angles but less or almost no effect at large-incidence angles. Compared with the numerical results under the fully developed wind seas, the sea states and swell waves finally affect the values of the simulated NBCSs at small- and medium-incidence angles but do not affect the variation trend of modulation effects by large-scale wave components on radar backscattering at different incidence angles.

To sum up, according to the examination of the effect of sea development states and swell waves on the radar backscattering from the wind sea, it is instructive for eliminating the inversion bias of sea surface wind speed due to sea states and swells from the radar measurements by configuring the appropriate radar parameters, such as high probing frequencies and large-incidence angles.

V. Conclusion

This study quantitatively investigated the effect of large-scale wave components relative to the Bragg component on radar backscattering from the multiscale sea surface using the SSA-1 model and Hwang sea wave spectrum as a function of incidence angles, wind speeds, and radar frequencies. The major findings of this study include the following.

The large-scale wave components ranging from 0 rad/m to $0.5K_{\text{Bragg}}$ rad/m have a significant effect of more than 3 dB on radar backscattering at small-incidence angles (i.e., less than 30°) under the moderate wind speed of 10 m/s, while their effect on NBCS weakens within 2 dB at medium-incidence angles of 30°–50°. The effect enhances with the increase of wind speed. However, as the incidence angle increases to 70°, these large-scale waves have an almost negligible effect on radar backscattering regardless of wind speed and radar frequency. This phenomenon can be physically explained by wavelength filtering. Only those roughness scales comparable to effective wavelength contribute to backscatter; other roughness scales are irrelevant and are inherently filtered out. This effect is also verified by AIEM and real measurement data. Consequently, the quantitative numerical analysis in this study improves our understanding of the effect of different large-scale waves on radar backscattering and can guide us to select the appropriate wave components for simulating the backscattering of sea surface and, thus, better-predicting microwave sea surface scatter.

Besides, the sea wave states and the swell waves can also cause some uncertainties to the NBCS simulation results, especially at low-frequency radar band (e.g., *L*-band) and at small-incidence angles (e.g., less than 30°), but they do not affect the variation trend of modulation effects by different large-scale wave components on the NBCS simulations at different incidence angles. More importantly, by examining the uncertainties caused by sea states and swell waves on the radar backscattering from the wind sea, we can use the high probing frequencies and large-incidence angles to eliminate the inversion bias of sea surface wind speed from radar measurements.

Appendix

A pivotal formula for SSA-1 model without the coherent scattering components is expressed as follows [5], [13]:

$$\sigma_{pq}^{0}\left(\mathbf{k}_i,\mathbf{k}_s\right)=\frac{1}{\pi}\left|\frac{2q_iq_sB_{pq}\left(\mathbf{k}_i,\mathbf{k}_s\right)}{Q}\right|^2$$

$$\cdot \left\{ \int \langle \exp[jQ\,(z_2 - z_1)] \rangle \cdot \exp\left[j\,(\mathbf{k}_s - \mathbf{k}_i) \cdot \mathbf{r}\right] d\mathbf{r} - \int \langle \exp[jQz_2] \rangle \cdot \langle \exp[-jQz_1] \rangle \cdot \exp\left[j\,(\mathbf{k}_s - \mathbf{k}_i) \cdot \mathbf{r}\right] d\mathbf{r} \right\}. \tag{12}$$

For the ensemble average terms in (12), the result up to the second order is as follows:

$$\begin{aligned} &\langle \exp[jQ\,(z_2 - z_1)] \rangle - \langle \exp[jQz_2] \rangle \cdot \langle \exp[-jQz_1] \rangle \\ &\quad \approx \exp\left\{ \frac{1}{2!} \left[C_{20}(jQ)^2 + 2C_{11}(jQ)(-jQ) + C_{02}(-jQ)^2 \right] \right\} \\ &\qquad - \exp\left[\frac{1}{2!} C_{20}(jQ)^2 \right] \cdot \exp\left[\frac{1}{2!} C_{02}(-jQ)^2 \right] \end{aligned} \tag{13}$$

where the symbol $\langle \cdot \rangle$ represents the ensemble average, and C indicates the expectation of random variable of sea surface height z. They can be expressed in terms of mean square height σ_z^2 or the autocorrelation function of sea surface $\sigma_z^2 \rho(\mathbf{r})$ and the related mathematical derivation can also be seen in [11] and [34]. For arbitrary two points, z_1 and z_2, on rough surface, here, $C_{20} = \langle z_2 \cdot z_2 \rangle = \sigma_z^2$, $C_{02} = \langle z_1 \cdot z_1 \rangle = \sigma_z^2$, and $C_{11} = \langle z_2 \cdot z_1 \rangle = \sigma_z^2 \rho(\mathbf{r})$.

Thus, after a straightforward manipulation, (13) can be given by an expression involving the mean square height σ_z^2 and autocorrelation function $\sigma_z^2 \rho(\mathbf{r})$.

$$\begin{aligned} &\langle \exp[jQ\,(z_2 - z_1)] \rangle - \langle \exp[jQz_2] \rangle \langle \exp[-jQz_1] \rangle \\ &\quad = \exp\left\{ \sigma_z^2 Q^2 \left[\rho(\mathbf{r}) - 1 \right] \right\} - \exp(-\sigma_z^2 Q^2) \\ &\quad = \exp\left(-\sigma_z^2 Q^2 \right) \left\{ \exp\left[\sigma_z^2 Q^2 \rho(\mathbf{r}) \right] - 1 \right\}. \end{aligned} \tag{14}$$

We may apply a Taylor series expansion for the exponential term in curly braces in (14) as follows:

$$\left\{ \left[1 + \sum_{n=1}^{\infty} \frac{\left[\sigma_z^2 Q^2 \rho(\mathbf{r}) \right]^n}{n!} \right] - 1 \right\} = \sum_{n=1}^{\infty} \frac{\left[\sigma_z^2 Q^2 \rho(\mathbf{r}) \right]^n}{n!}. \tag{15}$$

After some lengthy but straightforward manipulations, we can rewrite (12) in a compact form

$$\begin{aligned} \sigma_{pq}^0 (\mathbf{k}_i, \mathbf{k}_s) &= \frac{1}{\pi} \left| \frac{2 q_i q_s B_{pq} (\mathbf{k}_i, \mathbf{k}_s)}{Q} \right|^2 \cdot \exp\left(-\sigma_z^2 Q^2 \right) \\ &\quad \cdot \left\{ \sum_{n=1}^{\infty} \frac{\left[\sigma_z^2 Q^2 \rho\,(\mathbf{r}) \right]^n}{n!} \right\} \exp\left[j\,(\mathbf{k}_s - \mathbf{k}_i) \cdot \mathbf{r} \right] d\mathbf{r} \\ &= 4\pi \cdot \left| \frac{2 q_i q_s B_{pq} (\mathbf{k}_i, \mathbf{k}_s)}{Q} \right|^2 \cdot \exp\left(-\sigma_z^2 Q^2 \right) \\ &\quad \cdot \sum_{n=1}^{\infty} \frac{\left(\sigma_z^2 Q^2 \right)^n}{n!} \cdot W^{(n)} (\mathbf{k}_s - \mathbf{k}_i) \end{aligned} \tag{16}$$

where

$$W^{(n)}(\mathbf{k}_s - \mathbf{k}_i) = \frac{1}{(2\pi)^2} \int_0^{\infty} \int_0^{2\pi} \rho^n(\mathbf{r}) \cdot \exp\left[j(\mathbf{k}_s - \mathbf{k}_i) \cdot \mathbf{r} \right] d\mathbf{r}. \tag{17}$$

For more details and the specific parameters of the SSA-1 model, readers are referred to [29], [30], [34], and [35].

REFERENCES

[1] D. E. Barrick and W. H. Peake, "A review of scattering from surfaces with different roughness scales," *Radio Sci.*, vol. 3, no. 8, pp. 865–868, Aug. 1968.

[2] T. Elfouhaily, B. Chapron, K. Katsaros, and D. Vandemark, "A unified directional spectrum for long and short wind-driven waves," *J. Geophys. Res.*, vol. 102, no. C7, pp. 15781–15796, Jul. 1997.

[3] M. A. Donelan, F. W. Dobson, S. D. Smith, and R. J. Anderson, "On the dependence of sea surface roughness on wave development," *J. Phys. Oceanogr.*, vol. 23, no. 9, pp. 2143–2149, Sep. 1993.

[4] G. R. Valenzuela, "Theories for the interaction of electromagnetic and oceanic waves—A review," *Boundary-Layer Meteorol.*, vol. 13, no. 14, pp. 61–85, Jan. 1978.

[5] T. M. Elfouhaily and C.-A. Guerin, "A critical survey of approximate scattering wave theories from random rough surfaces," *Waves Random Media*, vol. 14, no. 4, pp. R1–R40, Oct. 2004.

[6] C.-A. Guérin, G. Soriano, and B. Chapron, "The weighted curvature approximation in scattering from sea surfaces," *Waves Random Complex Media*, vol. 20, no. 3, pp. 364–384, Jul. 2010.

[7] F. T. Ulaby and D. Long, *Microwave Radar and Radiometric Remote Sensing*. Ann Arbor, MI, USA: Univ. Michigan Press, 2014.

[8] P. Beckmann and A. Spizzichino, *The Scattering of Electromagnetic Waves From Rough Surfaces*. Norwood, MA, USA: Artech House, 1987.

[9] S. O. Rice, "Reflection of electromagnetic waves from slightly rough surfaces," *Commun. Pure Appl. Math.*, vol. 4, no. 2/3, pp. 351–378, Aug. 1951.

[10] J. Wright, "A new model for sea clutter," *IEEE Trans. Antennas Propag.*, vol. AP-16, no. 2, pp. 217–223, Mar. 1968.

[11] A. K. Fung, *Microwave Scattering and Emission Models and Their Applications*. Norwood, MA, USA: Artech House, 1994.

[12] T.-D. Wu, K.-S. Chen, J. Shi, H.-W. Lee, and A. K. Fung, "A study of an AIEM model for bistatic scattering from randomly rough surfaces," *IEEE Trans. Geosci. Remote Sens.*, vol. 46, no. 9, pp. 2584–2598, Sep. 2008.

[13] A. Voronovich, "Small-slope approximation for electromagnetic wave scattering at a rough interface of two dielectric half-spaces," *Waves Random Media*, vol. 4, no. 3, pp. 337–367, Oct. 1994.

[14] K. F. Warnick and W. C. Chew, "Numerical simulation methods for rough surface scattering," *Waves Random Media*, vol. 11, no. 1, pp. R1–R30, Jan. 2001.

[15] G. Soriano and C.-A. Guérin, "A cutoff invariant two-scale model in electromagnetic scattering from sea surfaces," *IEEE Geosci. Remote Sens. Lett.*, vol. 5, no. 2, pp. 199–203, Apr. 2008.

[16] D. Xie, K.-S. Chen, and J. Zeng, "The frequency selective effect of radar backscattering from multiscale sea surface," *Remote Sens.*, vol. 11, no. 2, Jan. 2019, Art. no. 160.

[17] J. T. Johnson, R. T. Shin, J. A. Kong, L. Tsang, and K. Pak, "A numerical study of the composite surface model for ocean backscattering," *IEEE Trans. Geosci. Remote Sens.*, vol. 36, no. 1, pp. 72–83, Jan. 1998.

[18] Y. Du, J. Yin, S. Tan, J. Wang, and J. Yang, "A numerical study of roughness scale effects on ocean radar scattering using the second-order SSA and the moment method," *IEEE Trans. Geosci. Remote Sens.*, vol. 58, no. 10, pp. 6874–6887, Oct. 2020.

[19] A. T. Manninen, "Multiscale surface roughness and backscattering—Summary," *J. Electromagn. Waves Appl.*, vol. 11, no. 4, pp. 471–475, Jan. 1997.

[20] T. Qiao *et al.*, "Sea surface radar scattering at L-Band based on numerical solution of Maxwell's equations in 3-D (NMM3D)," *IEEE Trans. Geosci. Remote Sens.*, vol. 56, no. 6, pp. 3137–3147, Jun. 2018.

[21] R. Romeiser, A. Schmidt, and W. Alpers, "A three-scale composite surface model for the ocean wave–radar modulation transfer function," *J. Geophys. Res., Oceans*, vol. 99, no. C5, pp. 9785–9801, May 1994.

[22] D. Lemaire, P. Sobieski, and A. Guissard, "Full-range sea surface spectrum in nonfully developed state for scattering calculations," *IEEE Trans. Geosci. Remote Sens.*, vol. 37, no. 2, pp. 1038–1051, Mar. 1999.

[23] W. J. Plant, "A stochastic, multiscale model of microwave backscatter from the ocean," *J. Geophys. Res., Oceans*, vol. 107, no. C9, pp. 3-1–3-21, Sep. 2002.

[24] V. Kudryavtsev, D. Hauser, G. Caudal, and B. Chapron, "A semiempirical model of the normalized radar cross-section of the sea surface 1: Background model," *J. Geophys. Res., Oceans*, vol. 108, no. C3, pp. FET 2-1–FET 2-24, Mar. 2003.

[25] P. A. Hwang and F. Fois, "Surface roughness and breaking wave properties retrieved from polarimetric microwave radar backscattering," *JGR Oceans*, vol. 120, no. 5, pp. 3640–3657, May 2015.
[26] G. D. Martino, A. Iodice, and D. Riccio, "Closed-form anisotropic polarimetric two-scale model for fast evaluation of sea surface backscattering," *IEEE Trans. Geosci. Remote Sens.*, vol. 57, no. 8, pp. 6182–6194, Aug. 2019.
[27] I. A. Sergievskaya *et al.*, "Modulation of dual-polarized X-band radar backscatter due to long wind waves," *Remote Sens.*, vol. 11, no. 4, Feb. 2019, Art. no. 423.
[28] A. G. Voronovich, "A two-scale model from the point of view of the small-slope approximation," *Waves Random Media*, vol. 6, no. 1, pp. 73–83, Jan. 1996.
[29] A. G. Voronovich and V. U. Zavorotny, "Theoretical model for scattering of radar signals in K_u- and C-bands from a rough sea surface with breaking waves," *Waves Random Media*, vol. 11, no. 3, pp. 247–269, Mar. 2001.
[30] A. G. Voronovich and V. U. Zavorotny, "Full-polarization modeling of monostatic and bistatic radar scattering from a rough sea surface," *IEEE Trans. Antennas Propag.*, vol. 62, no. 3, pp. 1362–1371, Mar. 2014.
[31] H. Zheng, J. Zhang, Y. Zhang, A. Khenchaf, and Y. Wang, "Theoretical study on microwave scattering mechanisms of sea surfaces covered with and without oil film for incidence angle smaller than 30°," *IEEE Trans. Geosci. Remote Sens.*, vol. 59, no. 1, pp. 37–46, Jan. 2021.
[32] H. Zheng, A. Khenchaf, Y. Wang, H. Ghanmi, Y. Zhang, and C. Zhao, "Sea surface monostatic and bistatic EM scattering using SSA-1 and UAVSAR data: Numerical evaluation and comparison using different sea spectra," *Remote Sens.,* vol. 10, no. 7, Jul. 2018, Art. no. 1084.
[33] J. Li, L. Wang, M. Zhang, W. Fan, and P. Wei, "Effective approach to generate electrically large rough surfaces and the application to EM scattering problems," *IET Microw., Antennas Propag.*, vol. 14, no. 4, pp. 233–240, Mar. 2020.
[34] C. Bourlier, "Azimuthal harmonic coefficients of the microwave backscattering from a non-Gaussian ocean surface with the first-order SSA model," *IEEE Trans. Geosci. Remote Sens.*, vol. 42, no. 11, pp. 2600–2611, Nov. 2004.
[35] A. G. Voronovich and V. U. Zavorotny, "The transition from weak to strong diffuse radar bistatic scattering from rough ocean surface," *IEEE Trans. Antennas Propag.*, vol. 65, no. 11, pp. 6029–6034, Nov. 2017.
[36] A. K. Fung, *Backscattering From Multiscale Rough Surfaces With Application to Wind Scatterometry*. Norwood, MA, USA: Artech House, 2015.
[37] P. A. Hwang and Y. Fan, "Low-frequency mean square slopes and dominant wave spectral properties: Toward tropical cyclone remote sensing," *IEEE Trans. Geosci. Remote Sens.*, vol. 56, no. 12, pp. 7359–7368, Dec. 2018.
[38] P. A. Hwang, Y. Fan, F. J. Ocampo-Torres, and H. García-Nava, "Ocean surface wave spectra inside tropical cyclones," *J. Phys. Oceanogr.*, vol. 47, no. 10, pp. 2393–2417, Oct. 2017.
[39] D. Xie, K.-S. Chen, and X. Yang, "Effects of wind wave spectra on radar backscatter from sea surface at different microwave bands: A numerical study," *IEEE Trans. Geosci. Remote Sens.*, vol. 57, no. 9, pp. 6325–6334, Sep. 2019.
[40] A. Stogryn, "Equations for calculating the dielectric constant of saline water (correspondence)," *IEEE Trans. Microw. Theory Techn.*, vol. MTT-19, no. 8, pp. 733–736, Aug. 1971.
[41] Y. Y. Yurovsky, V. N. Kudryavtsev, B. Chapron, and S. A. Grodsky, "Modulation of Ka-band doppler radar signals backscattered from the sea surface," *IEEE Trans. Geosci. Remote Sens.*, vol. 56, no. 5, pp. 2931–2948, May 2018.
[42] W. J. Plant, "Bragg scattering of electromagnetic waves from the air/sea interface," in *Surface Waves and Fluxes: Current Theory*, G. L. Geernaert and W. L. Plant, Eds. Dordrecht, The Netherlands: Kluwer, vol. 2, 1990, pp. 41–108.
[43] A. Guissard, "Multispectra for ocean-like random rough surface scattering," *J. Electromagn. Waves Appl.*, vol. 10, no. 10, pp. 1413–1443, Oct. 1996.
[44] G. Caulliez and C. A. Guérin, "Higher-order statistical analysis of short wind wave fields," *J. Geophys. Res., Oceans*, vol. 117, no. C6, Jun. 2012, Art. no. C06002.
[45] Y. Du, X. Yang, K.-S. Chen, W. Ma, and Z. Li, "An improved spectrum model for sea surface radar backscattering at L-band," *Remote Sens.,* vol. 9, no. 8, Jul. 2017, Art. no. 776.
[46] A. Stoffelen, J. A. Verspeek, J. Vogelzang, and A. Verhoef, "The CMOD7 geophysical model function for ASCAT and ERS wind retrievals," *IEEE J. Sel. Topics Appl. Earth Observ. Remote Sens.*, vol. 10, no. 5, pp. 2123–2134, May 2017.
[47] M. Ryabkova, V. Karaev, J. Guo, and Y. Titchenko, "A review of wave spectrum models as applied to the problem of radar probing of the sea surface," *JGR Oceans*, vol. 124, no. 10, pp. 7104–7134, Oct. 2019.
[48] Y. Liu, M.-Y. Su, X.-H. Yan, and W. T. Liu, "The mean-square slope of ocean surface waves and its effects on radar backscatter," *J. Atmos. Ocean. Technol.*, vol. 17, pp. 1092–1105, Aug. 2000.
[49] Y. Cheng *et al.*, "An analytical algorithm with a wave age factor for altimeter wind speed retrieval," *Int. J. Remote Sens.*, vol. 29, pp. 5699–5716, Sep. 2008.
[50] S. Li, B. Liu, H. Shen, Y. Hou, and W. Perrie, "Wind wave effects on remote sensing of sea surface currents from SAR," *JGR Oceans*, vol. 125, no. 7, Jul. 2020, Art. no. e2020JC016166.
[51] P. A. Hwang, J. D. Ouellette, J. V. Toporkov, and J. T. Johnson, "A simulation study of significant wave height retrieval from bistatic scattering of signals of opportunity," *IEEE Geosci. Remote Sens. Lett.*, vol. 19, 2022, Art. no. 8017205.
[52] S. I. Badulin, V. G. Grigorieva, P. A. Shabanov, V. D. Sharmar, and I. O. Karpov, "Sea state bias in altimetry measurements within the theory of similarity for wind-driven seas," *Adv. Space Res.*, vol. 68, no. 2, pp. 978–988, Jul. 2021.
[53] C. Lucas and C. G. Soares, "On the modelling of swell spectra," *Ocean Eng.,* vol. 108, no. 8, pp. 749–759, Nov. 2015.
[54] S. Durden and J. Vesecky, "A physical radar cross-section model for a wind-driven sea with swell," *IEEE J. Ocean. Eng.*, vol. OE-10, no. 4, pp. 445–451, Oct. 1985.
[55] J. E. Stopa, A. A. Mouche, B. Chapron, and F. Collard, "Sea state impacts on wind speed retrievals from C-band radars," *IEEE J. Sel. Topics Appl. Earth Observ. Remote Sens.*, vol. 10, no. 5, pp. 2147–2155, May 2017.
[56] H. Li, A. Mouche, and J. E. Stopa, "Impact of sea state on wind retrieval from sentinel-1 wave mode data," *IEEE J. Sel. Topics Appl. Earth Observ. Remote Sens.*, vol. 12, no. 2, pp. 559–566, Feb. 2019.
[57] H. Jiang, H. Zheng, and L. Mu, "Improving altimeter wind speed retrievals using ocean wave parameters," *IEEE J. Sel. Topics Appl. Earth Observ. Remote Sens.*, vol. 13, pp. 1917–1924, May 2020.
[58] P. A. Hwang and W. J. Plant, "An analysis of the effects of swell and surface roughness spectra on microwave backscatter from the ocean," *J. Geophys. Res.*, vol. 115, no. C4, Apr. 2010, Art. no. C04014.

Dengfeng Xie received the B.S. degree in land resource management from Chang'an University, Xi'an, China, in 2013, the M.S. degree in cartography and geographical information system from Beijing Normal University, Beijing, China, in 2016, and the Ph.D. degree in cartography and geographical information system from the Institute of Remote Sensing and Digital Earth, Chinese Academy of Science, Beijing, China, and the University of Chinese Academy of Science, Beijing, China, in 2019.

He is currently a Lecturer with the School of Geomatics Science and Technology, Nanjing Tech University, Nanjing, China. His current research interests include electromagnetic signal and scattering from the ocean.

Feng Guo received the B.S. degree in geographic information science in 2022 from Nanjing Tech University, Nanjing, China, where he is currently working toward the master's degree in the retrieval of sea surface wind field based on GNSS-R technology.

His research interests include the applications of GNSS-R in marine environment monitoring.